

Vessel segmentation in retinal images with a multiple kernel learning based method

Xiaoming Liu, Zhigang Zeng, Xiaoping Wang

Abstract—Blood vessel segmentation is an important problem for quantitative structure analysis of retinal images, and many diseases are related to the structure changes. Manual segmentation is time consuming and computer aided segmentation is required to deal with large amount images. This paper presents a new supervised method for segmentation of blood vessels in retinal photographs. Multiple kernel learning (MKL) is introduced to deal with the problem, utilizing features from Hessian matrix based vesselness measure, response of multiscale Gabor filter, and multiple scale line strength features. The method is evaluated on the publicly available DRIVE and STARE databases. The performance of the MKL method is evaluated and experimental results show the high accuracy of the proposed method.

I. INTRODUCTION

Changes in retinal blood vessel structures may reveal several serious diseases, such as diabetes, hypertension, cardiovascular disease and stroke. For example, changes in vessel caliber, branching angle or vessel tortuosity are results of hypertension [1]. The abnormal growth of new blood vessels in retinal is a sign of diabetic retinopathy [2], which is the leading cause of blindness in developed countries. The presence of arteriovenous nicking is an important precursor of stroke [3]. The early detection of these changes is very important in order to perform early intervention and prevent the patients from major vision loss. Vessel segmentation is a critical step for quantitative analysis of these changes. Location of the vessels can help to reduce the number of false positives in the detection of microaneurysms [4], can be used as a means for registration of images taken at different time [5], and can help to find optic disk and the fovea in retinal images.

However, manual segmentation of blood vessel is labor intensive and time consuming, especially when the number of images needing process is large. Thus, automatic vessel segmentation has received great attentions and several methods have been proposed. A complete review of existing methods for retinal blood vessel segmentation can be referred to [6].

Xiaoming Liu, Zhigang Zeng and Xiaoping Wang are with the School of Automation, Huazhong University of Science and Technology, Wuhan 430074, China, Key Laboratory of Image Information Processing and Intelligent Control, Ministry of Education, Wuhan 430074, China, E-mail: hustzgzeng@gmail.com

Xiaoming Liu is also with College of Computer Science and Technology, Wuhan University of Science and Technology, Wuhan 430081, China; Hubei Province Key Laboratory of Intelligent Information Processing and Real-time Industrial System, Wuhan, China

This work was supported by Natural Science Foundation of China (NO. 31201121, NO. 61273303, NO. 61100055), Educational Commission of Hubei Province (NO. D20131101).

Liu et al. [7] proposed a recursive tracking method to detect vasculature in retinal angiograms, which starts from some seed points and following the vessel center line guided by local information. Once a segment has been tracked, it is deleted in the angiogram image by growing the deletion in intensity value over the gray levels representing the vessel. Yin et al. [8] utilized a Bayesian based tracking method for vessel segmentation.

Based on the assumption that the intensity profile along the cross-section of a vessel has a typical shape, such as Gaussian, matched filter methods have been utilized by Chaudhuri et al. [9] for vessel detection. Hoover et al. [10] combined local and region-based properties of retinal blood vessels for segmentation using a threshold probing technique on a matched filter response image generated by the method in [9].

Recently, several supervised methods have been proposed to deal with the vessel segmentation problem [11], [12], [13], [14]. In these methods, each image pixel is represented by a feature vector, computed to represent local or global information of the image. A supervised classifier, such as artificial neural networks, K nearest neighbors, support vector machines (SVM), is then used classify each pixel as vessel or non-vessel after training with known samples. These methods could achieve higher accuracy than other unsupervised methods with the help of training samples.

In this paper, a new supervised method for segmentation of blood vessels by using multiple kernel support vector machine (MK SVM) is proposed. Although multiple kernel learning (MKL) method [15] has been widely used for pattern recognition, as far as the authors know, this is the first time of applying MKL for the segmentation of vessels in retinal image. The following features are used, the Vesselness measure proposed by Frangi [16], multiscale gabor response [12], multiple scale line strength features [17], and the original inverted green channel grayscale value.

The organization of this paper is as follows. In Section II, the features used in the method are introduced and the MK SVM method is brief introduced in Section III. The performance of the method is presented in Section IV. And the paper is concluded in Section V.

II. EXTRACTED FEATURES

The image pixels of a fundus image will be represented by feature vectors, and statistical classifiers is used in order to segment the image. In our case, two classes (vessel or nonvessel) are involved. The training set for the classifier comes from manual segmentations of training images, i.e.,

pixels segmented by hand are labeled as vessel while the remaining pixels are labeled as nonvessel.

Eight features are used to represent each pixel, which includes: Frangi vesselness (2 features), the Gabor filter response at multiple scales (4 features), and multiscale line operator response (1 feature), and the original green inverted grayscale value (1 feature).

1) Frangi vesselness (2 features) [16]: It uses values derived from image Hessian matrix analysis. The numerical estimation of the Hessian of the intensity image I in the scale space at a point (x, y) is:

$$H(x, y) = \begin{bmatrix} \frac{\partial^2 I}{\partial x^2} & \frac{\partial^2 I}{\partial x \partial y} \\ \frac{\partial^2 I}{\partial y \partial x} & \frac{\partial^2 I}{\partial y^2} \end{bmatrix} = \begin{bmatrix} I_{xx} & I_{xy} \\ I_{yx} & I_{yy} \end{bmatrix} \quad (1)$$

The partial derivatives are computed by convolving the intensity function with the first derivatives of a Gaussian kernel. A ridgeness score R_B is computed as the ratio of the eigenvalues of the Hessian, λ_1, λ_2 , with $|\lambda_1| \leq |\lambda_2|$. The score is defined as $R_B = \frac{\lambda_1}{\lambda_2}$. The vesselness measure is defined by

$$\nu_0 = \begin{cases} 0, & \lambda_2 > 0 \\ \exp\left(-\frac{R^2}{2\beta^2}\right) \left(1 - \exp\left(-\frac{S^2}{2c^2}\right)\right), & \text{otherwise} \end{cases} \quad (2)$$

where S is the Frobenius norm of the Hessian,

$$S = \|H\|_F = \sqrt{\lambda_1^2 + \lambda_2^2} \quad (3)$$

β , and c are two weights that control the sensitivity of the filter, $\beta = 0.5$ and c is set to half of the maximum Frobenius norm of the Hessian computed on the whole image.

In the background where no structure or contrast is present, the Frobenius norm of the Hessian is low, on the other hand, when vessel structure is present, the Frobenius norm will be large, since one of the eigenvalues is large. Therefore, S is also used to distinguish between background and vessel pixels. See Fig.1 for examples of Frangi vesselness on STARE and DRIVE images.

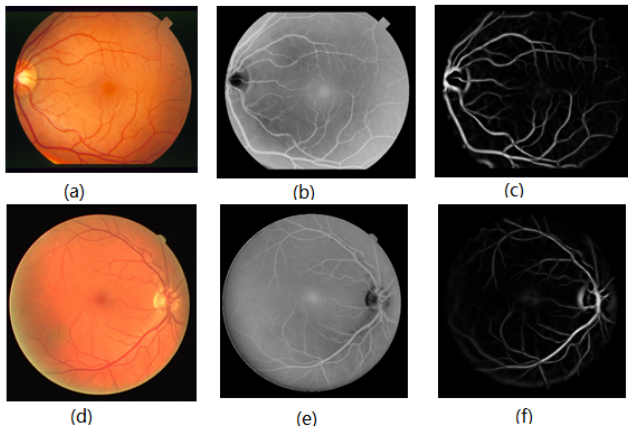


Fig. 1. Vesselness measure examples. (a) a color image in STARE, (b) inverted green channel image of (a), (c) Frangi vesselness of (b); (d) a color image in DRIVE, (e) inverted green channel image of (d), (f) Frangi vesselness of (e)

2) Multiscale Gabor Filter (4 features) [12]. Gabor filter has been widely used in several applications for multiscale and multidirectional edge detection. The Gabor filter can be fine-tuned to particular frequencies, scales and directions. The impulse response of a Gabor filter kernel is defined by the product of a Gaussian kernel and a complex sinusoid. It can be expressed as

$$g(x, y) = \exp\left\{-0.5\left(\frac{x'^2 + \gamma y'^2}{2\sigma^2}\right)\right\} \exp\{i(2\pi f x' + \psi)\} \quad (4)$$

where f is the modulation frequency of the complex sinusoid, ψ is the phase offset, σ is the scale of the Gaussian envelope, γ is the spatial aspect ratio, $x' = x \cos \theta + y \sin \theta$, and $y' = -x \sin \theta + y \cos \theta$ with orientation θ .

The Gabor filter response is obtained by a 2D convolution operator with FFT computation in the frequency domain. Four scales ($\sigma = 2, 3, 4, 5$) are used in the paper, and 4 features are extracted for each pixel. For each scale, filter responses of 18 orientation are computed (with θ spans from 0° to 170° with increment of 10°), and the maximum is taken as the feature of the specific scale. Fig.2 shows the Gabor filter response of example images.

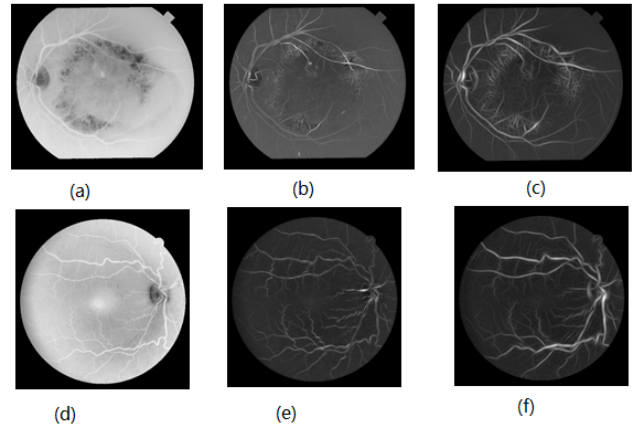


Fig. 2. Multiscale Gabor filter. (a) a green channel inverted image in STARE, (b) Gabor filter response of (a) with scale 2, (c) Gabor filter response of (a) with scale 5. (d) a green channel inverted image in DRIVE, (e) Gabor filter response of (d) with scale 2, (f) Gabor filter response of (d) with scale 5.

3) Multiple Scale Line Strength Features (1 feature) [17]. The retinal vasculature can be approximated with piecewise linear features, with variable width. Based on this observation, Ricci et al. [17] has used linear operator and morphological attributes to segment blood vessels in retinal images.

At each pixel position, a window of size $W \times W$ pixels centered on the pixel is identified and the average gray level is computed as I_{avg}^W . Twelve lines of length W pixels oriented at 12 different directions also centered on the pixel are identified and the average of gray levels of pixels along each line are computed. Denote the maximum average value among these 12 lines as I_{max}^L , and the line response at a

pixel is then computed as

$$R_W = I_{max}^L - I_{avg}^W \quad (5)$$

In [13], a fixed length of 15 pixels is used. As long length line detectors can deal with central reflex problem in retinal images, they tend to merge close vessels and produce false positives along the vessels. While short length line detectors can avoid wrongly merge of close vessels, they may introduce background noise in the image. To combine their advantages and avoid disadvantages. The fixed length line detection method has been further extended to multi-scale line detection [17], [18]. In this paper, the line responses at 8 scales (from 1 to 15 with a step 2) are linearly combined to get the final response, as in [17]. See Fig.3 for an example.

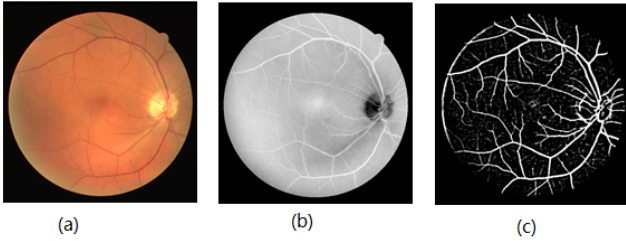


Fig. 3. Multiple scale line strength features example. (a) original image in DRIVE, (b) green channel inverted image, (c) multiple scale line strength feature.

III. MULTIPLE KERNEL SVM CLASSIFIER

MKL [15] is investigated for the classification, which extends SVM with multiple kernel. SVM algorithms were developed based on statistical pattern recognition theory, and they are considered capable of achieving better performance than neural networks, C4.5 in terms of accuracy and computational complexity for many binary classification problems. Given pairs of training examples $\{(x_i, y_i)\}_{i=1}^n$ where $x_i \in X$ and $y_i \in \{-1, +1\}$. Each x is mapped to a $\phi(x)$ by the kernel function K with $K(x_i, x_j) = \phi(x_i)^T \phi(x_j)$ for any $x_i, x_j \in X$. Then, the optimization problem in SVM is

$$\begin{aligned} \min_{w, b, \xi} & \frac{1}{2} \|w\|^2 + C \sum_{i=1}^n \xi_i \\ \text{s.t.} & y_i (w^T \phi(x_i) + b) \geq 1 - \xi_i, \\ & \xi_i \geq 0, i = 1, 2, \dots, n \end{aligned} \quad (6)$$

where ξ_1, \dots, ξ_n are the slack variables for the errors and C is a user defined regularization parameter that trades off the margin with error. The final classification for a new sample x is

$$y = \text{sgn} \left(\sum_{i=1}^n n w_i K(x, x_i) + b \right) \quad (7)$$

Unlike SVM with a single kernel K , in the MKL method, we have a set of M base kernels K_1, \dots, K_M , with the corresponding kernel induced feature maps ϕ_1, \dots, ϕ_M . The optimization problem of MKL can be formulated as [15]:

$$\begin{aligned} \min_{w, b, \xi} & \frac{1}{2} \sum_{i=1}^M \|w\|^2 + C \sum_{i=1}^n \xi_i \\ \text{s.t.} & y_i \left(\sum_{k=1}^M w_k^T \phi_k(x_i) + b \right) \geq 1 - \xi_i, \\ & \xi_i \geq 0, i = 1, 2, \dots, n \end{aligned} \quad (8)$$

where w_k is the weight for component ϕ_k . The final kernel in MKL is formed by a convex combination of the kernels

$$K = \sum_{k=1}^M u_k K_k \quad (9)$$

the relation between w and u is:

$$w_k = u_k \sum_{i=1}^n \alpha_i y_i \phi_k(x_i) \quad (10)$$

where $0 \leq \alpha_i \leq C$, and

$$u_k \geq 0, \sum_{k=1}^M u_k = 1 \quad (11)$$

For more details please refer to [15]. MKL has been widely used in several applications and showing better performance over SVM.

IV. EXPERIMENTAL RESULTS

The method has been evaluated using two public available databases (STARE and DRIVE). The DRIVE database [11] contains 40 color images of the retina along with manual segmentation of vessels. These images are captured using a Canon CR5-3CCD camera at 45° field of view (FOV). The size of images is 565×584 pixels and used 8 bits in each color channel. The image set is divided into training and test set, each of them contains 20 images. The images in the training set are marked by one observer, and the images in the test set are marked by two observers. The first observer marked 12.7% pixels as vessel, and the second observer marked 12.3% pixels as vessel. The first marker is used as ground truth.

The STARE database [10] contains 20 colored retinal images, among them 10 images contain pathologies. The images are captured by a TopCon TRV-50 fundus camera at 35° FOV. The size of images is 700×605 pixels, with 24 bits per pixel (standard RGB). The FOV in the images is approximately 650×550 pixels. Each image is manual segmented by two observers. The first observer marked 10.4% of pixels as vessel, the second one marked 14.9%. The segmentation of the first observer is used as ground truth.

The classification performance is measured with true positive rate (TPR), false positive rate (FPR), and accuracy. Denote the true positive number of a classifier to be TP , false positive number to be FP , true negative number to be TN , and false negative number to be FN , then TPR is defined as

$$TPR = \frac{TP}{TP + FN} \quad (12)$$

FPR is defined as

$$FPR = \frac{FP}{FP + TN} \quad (13)$$

Accuracy (ACC) is defined as

$$ACC = \frac{TP + TN}{TP + FP + TN + FN} \quad (14)$$

TABLE I
VESSEL EXTRACTION PERFORMANCES ON DRIVE DATASET

Method	TPR	FPR	Average Accuracy
Chauduri et al. [9]	0.6168	0.0259	0.9284
Staal et al. [11]	0.6780	0.0170	0.9441
Mendonca et al. [19]	0.7344	0.0236	0.9452
Martinez-Perez et al. [20]	0.7246	0.0345	0.9344
Our method (MKL)	0.7352	0.0226	0.9467

TABLE II
VESSEL EXTRACTION PERFORMANCES ON STARE DATASET

Method	TPR	FPR	Average Accuracy
Normal cases			
Chauduri et al. [9]	0.7335	0.0218	0.9486
Hoover et al. [10]	0.6766	0.0338	0.9324
Soares et al. [12]	0.7554	0.0188	0.9542
Our method (MKL)	0.7822	0.0214	0.9619
Abnormal cases			
Chauduri et al. [9]	0.5881	0.0384	0.9227
Hoover et al. [10]	0.6736	0.0528	0.9211
Soares et al. [12]	0.6869	0.0318	0.9416
Our method (MKL)	0.7432	0.0362	0.9516

For the SVM kernel, 10 RBF kernels are investigated, while other kernels such as polynomial kernels may also be used. The performance comparison of our method with other approaches in terms of TPR, FPR and accuracy is shown in Table 1 and Table 2. Fig.4 shows several segmentations of our method on DRIVE dataset, and results on STARE are shown in Fig.5. The algorithm was performed on a workstation with Intel Core 2 Duo CPU 2.4G and 4G RAM. The time required to process a single image is less than two minutes and thirty seconds. From the figures and tables, it can be seen that our method achieved better performance than other methods. On the DRIVE, an accuracy of 0.9467 is obtained and an accuracy of 0.9568 is obtained on STARE dataset. Especially on pathology cases in STARE dataset, the TPR is increased from 0.6869 to 0.7432, which indicates that our method is less affected by pathology features. MKL outperforms traditional SVM in our application may due to it can handle different characteristics of features by integrating several kernels.

V. CONCLUSIONS

In this paper, an effective multiple kernel learning based retinal segmentation method is proposed. Several features are used in the method, obtained from Frangi vesselness measurement (2 features), Multiscale Gabor Filter (4 features), Multiple Scale Line Strength Features (1 feature), and the inverted green channel grayscale value (1 feature). On DRIVE dataset, an accuracy of 94.67% is achieved, and 95.68% is achieved on STARE dataset, which is comparable or better than several previous methods. In the future, we plan to investigate more features and to improve further the accuracy of the method.

REFERENCES

[1] T.Y. Wong and R. McIntosh, "Hypertensive retinopathy signs as risk indicators of cardiovascular morbidity and mortality," *British Medical Bulletin*, vol. 73, no. 1, pp.57-70, 2005.

[2] E.J. Sussman, W.G. Tsiaras and K.A. Soper, "Diagnosis of diabetic eye disease," *The Journal of the American Medical Association*, vol. 247, no. 23, pp. 3231-3234, 1982.

[3] N. Patton, T.M. Aslam, T. MacGillivray, I.J. Deary, B. Dhillon, R.H. Eikelboom, K. Yogesan and I.J. Constable, "Retinal image analysis: concepts, applications and potential Progress in Retinal and Eye Research," *Progress in Retinal and Eye Research*, vol. 25, no. 1, pp. 99-127, 2006.

[4] A.J. Frame, P.E. Undrill, M.J. Cree, J.A. Olson, K.C. McHardy, P.F. Sharp and J.V. Forrester, "A comparison of computer based classification methods applied to the detection of microaneurysms in ophthalmic fluorescein angiograms," *Computers in Biology and Medicine*, vol. 28, no. 3, pp. 225-238, 1998.

[5] F. Zana and J.C. Klein, "A multimodal registration algorithm of eye fundus images using vessels detection and Hough transform," *IEEE Transactions on Medical Imaging*, vol. 18, no. 5, pp. 419-428, 1999.

[6] M.M. Fraz, P. Remagnino, A. Hoppe, B. Uyyanonvara, A.R. Rudnicka, C.G. Owen and S.A. Barman, "Blood vessel segmentation methodologies in retinal images—A survey," *Computer Methods and Programs in Biomedicine*, vol. 108, no. 1, pp. 407-433, 2012.

[7] I. Liu and Y. Sun, "Recursive tracking of vascular networks in angiograms based on the detection-deletion scheme," *IEEE Transactions on Medical Imaging*, vol. 12, no. 2, pp. 334-341, 1993.

[8] Y. Yin, M. Adel and S. Bourenane, "Retinal vessel segmentation using a probabilistic tracking method," *Pattern Recognition*, vol. 45, no. 4, pp. 1235-1244, 2012.

[9] S. Chaudhuri, S. Chatterjee, N. Katz, M. Nelson and M. Goldbaum, "Detection of blood vessels in retinal images using two-dimensional matched filters," *IEEE Transactions on Medical Imaging*, vol. 8, no. 3, pp. 263-269, 1989.

[10] A. Hoover, V. Kouznetsova and M. Goldbaum, "Locating blood vessels in retinal images by piecewise threshold probing of a matched filter response," *IEEE Transactions on Medical Imaging*, vol. 19, no. 3, pp. 203-210, 2000.

[11] J. Staal, M.D. Abramoff, M. Niemeijer, M.A. Viergever and B. van Ginneken, "Ridge-based vessel segmentation in color images of the retina," *IEEE Transactions on Medical Imaging*, vol. 23, no. 4, pp. 501-509, 2004.

[12] J.V. Soares, J.J. Leandro, R.M. Cesar, H.F. Jelinek and M.J. Cree, "Retinal vessel segmentation using the 2-D Gabor wavelet and supervised classification," *IEEE Transactions on Medical Imaging*, vol. 25, no. 9, pp. 1214-1222, 2006.

[13] E. Ricci and R. Perfetti, "Retinal blood vessel segmentation using line operators and support vector classification," *IEEE Transactions on Medical Imaging*, vol. 26, no. 10, pp. 1357-1365, 2007.

[14] D. Marin, A. Aquino, M.E. Gegndez-Arias and J.M. Bravo, "A new supervised method for blood vessel segmentation in retinal images by using gray-level and moment invariants-based features," *IEEE Transactions on Medical Imaging*, vol. 30, no. 1, pp. 146-158, 2011.

[15] F.R. Bach, G.R. Lanckriet and M.I. Jordan, "Multiple kernel learning, conic duality, and the SMO algorithm," *Proceedings of the Twenty-first International Conference on Machine Learning*, 2004.

[16] A.F. Frangi, W.J. Niessen, K.L. Vincken and M.A. Viergever, "Multiscale vessel enhancement filtering," *Medical Image Computing and Computer-Assisted Intervention MICCAI98*, Springer, 130-137, 1998.

[17] U.T.V. Nguyen, A. Bhuiyan, L.A.F. Park and K. Ramamohanarao, "An effective retinal blood vessel segmentation method using multi-scale line detection," *Pattern Recognition*, vol. 46, no. 3, pp. 703-715, 2013.

[18] D.J. Farnell, F. Hatfield, P. Knox, M. Reakes, S. Spencer, D. Parry and S.P. Harding, "Enhancement of blood vessels in digital fundus photographs via the application of multiscale line operators," *Journal of the Franklin Institute*, vol. 345, no. 7, pp. 748-765, 2008.

[19] A.M. Mendonca and A. Campilho, "Segmentation of retinal blood vessels by combining the detection of centerlines and morphological reconstruction," *IEEE Transactions on Medical Imaging*, vol. 25, no. 9, pp. 1200-1213, 2006.

[20] M.E. Martinez-Perez, A.D. Hughes, S.A. Thom, A.A. Bharath and K.H. Parker, "Segmentation of blood vessels from red-free and fluorescein retinal images", *Medical Image Analysis*, vol. 11, no. 1, pp. 47-61, 2007.

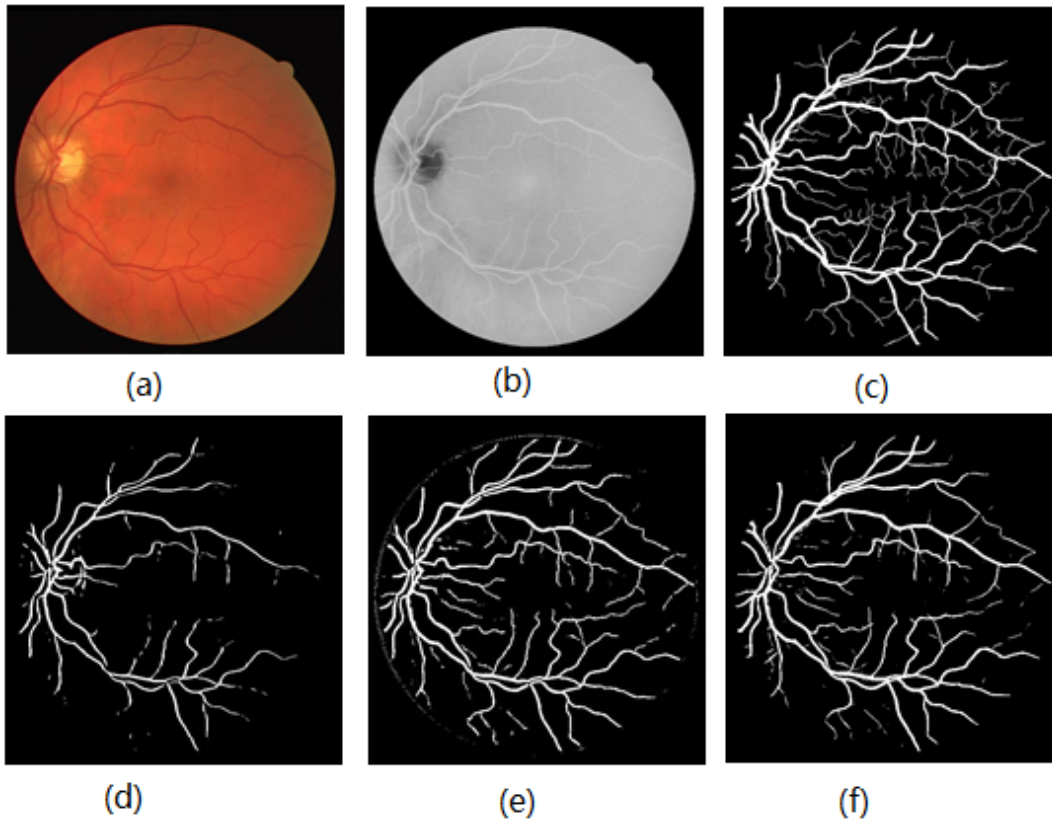


Fig. 4. Segmentation result of an image in DRIVE. (a) original color image, (b) green channel inverted image, (c) manual segmentation result, (d) result of Chaudhuri method, (e) result of Staal result, (f) result of the proposed method.

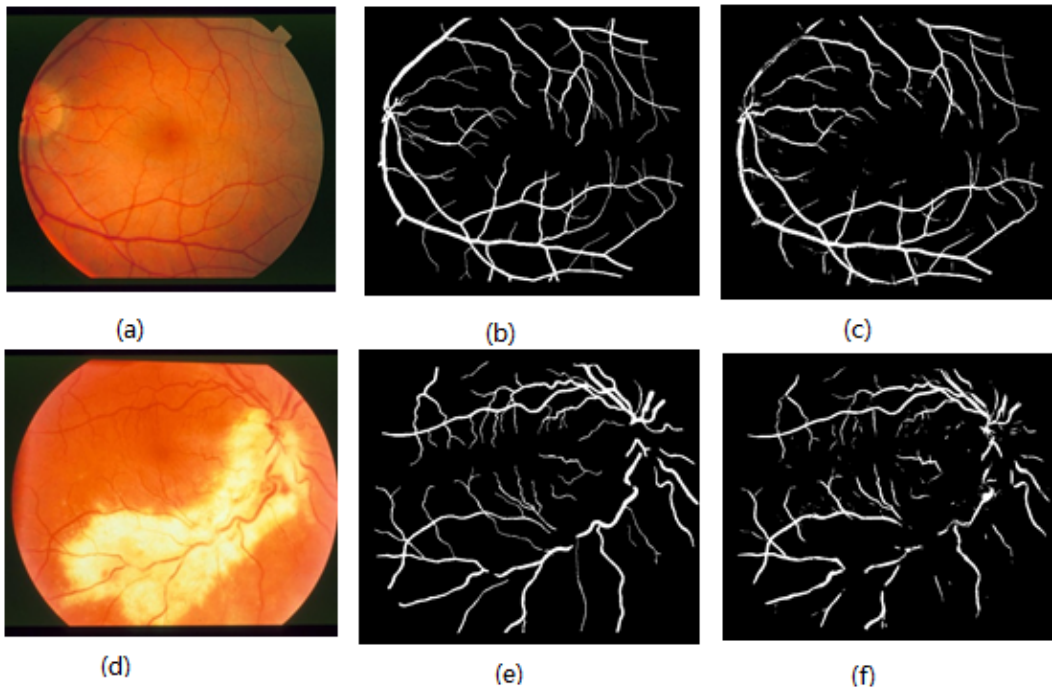


Fig. 5. Results on STARE. (a) original image of an image, (b) manual segmentation of (a), (c) our result on (a), (d) another image, (e) manual segmentation of (d), (f) our result on (d).